

Reconstructing chromosphere concentration images directly by continuous-wave diffuse optical tomography

Ang Li

*Martinos Center for Biomedical Imaging, Massachusetts General Hospital, Harvard Medical School,
Charlestown, Massachusetts 02129, and
Department of Physics, Tufts University, Medford, Massachusetts 02155*

Quan Zhang and Joseph P. Culver

Martinos Center for Biomedical Imaging, Massachusetts General Hospital, Harvard Medical School, Charlestown, Massachusetts 02129

Eric L. Miller

Department of Electrical and Computer Engineering, Northeastern University, Boston, Massachusetts 02115

David A. Boas

Martinos Center for Biomedical Imaging, Massachusetts General Hospital, Harvard Medical School, Charlestown, Massachusetts 02129

Received August 1, 2003

We present an algorithm to reconstruct chromosphere concentration images directly rather than following the traditional two-step process of reconstructing wavelength-dependent absorption coefficient images and then calculating chromosphere concentration images. This procedure imposes prior spectral information into the image reconstruction that results in a dramatic improvement in the image contrast-to-noise ratio of better than 100%. We demonstrate this improvement with simulations and a dynamic blood phantom experiment.

© 2004 Optical Society of America

OCIS codes: 170.3880, 220.0220, 220.4000, 170.3010.

Diffuse optical tomography is used to image the changes in the concentration of oxyhemoglobin (HbO₂) and deoxyhemoglobin (HbR) in tissue.^{1,2} The technique exploits the fact that HbO₂ and HbR are the dominant absorbers in the infrared region (650–950 nm). In a typical reconstruction scheme there are three steps to get the final HbO₂ and HbR images. First, the measurements are taken simultaneously at two or more different wavelengths. Second, images of the absorption coefficients at the different wavelengths are reconstructed separately. Finally, the concentration of the HbO₂ and HbR are calculated from the spectral variation in the absorption images. Because of the ill-posed nature of the diffuse optical tomography inverse problem, however, the optical images are highly sensitive to measurement noise and systematic model error,³ thereby amplifying the image noise when we calculate HbO₂ and HbR from optical imaging.

In the new technique we present here, images of HbO₂ and HbR are reconstructed directly instead of first reconstructing the spectral absorption images, as also suggested by others.^{4–6} In this way we expect to suppress image noise and reduce cross talk in the HbO₂ and HbR images by forcing spectral consistency in the reconstructed images. We demonstrate the expected improvement with simulations and a phantom experiment.

Near-infrared (650–950-nm) light propagation in tissue is well approximated over long distances by the diffusion equation.⁷ Within the limit in which spatial changes in absorption (μ_a) and scattering (μ_s') coefficients are small, we can linearize the equation and find solutions using appropriate Green's functions.³ By simulation and the phantom results shown here, we assume that μ_s' is constant. We adopt a first-order

perturbation solution Φ_1 to solve the diffusion equation. Solutions for Φ_1 for different boundary conditions can be found in Refs. 8 and 9. The important fact is that the solution is wavelength dependent. The wavelength dependence of the optical properties is directly related to physiology parameters. For example, if the absorption is dominated by hemoglobin then

$$\mu_a(\lambda) = \epsilon_{\text{HbO}_2}(\lambda)[\text{HbO}_2] + \epsilon_{\text{HbR}}(\lambda)[\text{HbR}], \quad (1)$$

where ϵ represents the extinction coefficients of HbO₂ and HbR, which are wavelength dependent, and the [X] indicates the concentration of X. To obtain a unique solution of [HbO₂] and [HbR], we need measurements of at least two different wavelengths.

Making use of Eq. (1) allows us to write Φ_1 at two different wavelengths directly in terms of the unknown perturbations to the HbO₂ and HbR concentrations:

$$\begin{bmatrix} \Phi_1(\lambda_1) \\ \Phi_1(\lambda_2) \end{bmatrix} = \begin{bmatrix} W(\lambda_1) & 0 \\ 0 & W(\lambda_2) \end{bmatrix} \begin{bmatrix} \delta\mu_a(\lambda_1) \\ \delta\mu_a(\lambda_2) \end{bmatrix} \quad (2a)$$

$$= \begin{bmatrix} \epsilon_{\text{HbO}_2}(\lambda_1)W(\lambda_1) & \epsilon_{\text{HbR}}(\lambda_1)W(\lambda_1) \\ \epsilon_{\text{HbO}_2}(\lambda_2)W(\lambda_2) & \epsilon_{\text{HbR}}(\lambda_2)W(\lambda_2) \end{bmatrix} \times \begin{pmatrix} \delta[\text{HbO}_2] \\ \delta[\text{HbR}] \end{pmatrix}. \quad (2b)$$

Here, $\Phi_1(\lambda_1)$ and $\Phi_1(\lambda_2)$ are column vectors of the measured perturbation at λ_1 and λ_2 , where each element in the vector represents a measurement with a different source–detector pair. The measured perturbation arises from spatial variation in the absorption coefficient at each wavelength as indicated by the vectors

$\delta\mu_a(\lambda_1)$ and $\delta\mu_a(\lambda_2)$, where each vector element represents an individual element in the highly scattering medium. The transformation from the spatial variation in the absorption coefficient to the measured perturbation at each wavelength is given by the weight matrices $W(\lambda_1)$ and $W(\lambda_2)$.³ Substitution of Eq. (1) into Eq. (2a) results in Eq. (2b). It is through inversion of the matrix in Eq. (2b) that we are able to reconstruct images of the physiological parameters [HbO₂] and [HbR] directly.

Since the weight matrix is usually ill-conditioned and underdetermined, we utilize the regularized Moore–Penrose generalized inverse solution $x = A^T(AA^T + \beta I)^{-1}y$ for the problem $y = Ax$ [as formulated in Eq. (2)], where the regularization parameter $\beta = \alpha \max(AA^T)$, and α is varied to optimize the image trade-off between resolution and noise. After calculating the optical images $\delta\mu_a(\lambda_1)$ and $\delta\mu_a(\lambda_2)$ by use of Eq. (2a), one typically combines the images using Eq. (1) to obtain the physiological images $\delta[\text{HbO}_2]$ and $\delta[\text{HbR}]$. Our novel approach is to reconstruct images of $\delta[\text{HbO}_2]$ and $\delta[\text{HbR}]$ directly utilizing Eq. (2b). To explore the difference between the two approaches, simulations were performed in a 6-cm-thick slab geometry. The optical properties of the phantom were $\mu_s' = [5.0, 4.5, 4.0] \text{ cm}^{-1}$ and $\mu_a = [0.01, 0.02, 0.025] \text{ cm}^{-1}$ at wavelengths of [690, 780, 830] nm, respectively. These are commonly available laser diode wavelengths. A spherical heterogeneity with a radius of 1 cm having a 0- μM HbO₂ concentration and a 28- μM HbR concentration inside was positioned in the center of the otherwise homogeneous medium. Nine continuous-wave sources and nine detectors were positioned on opposing 3×3 grids with a 2-cm spacing to collect transmitted data. We chose two sets of wavelengths: grouping A (690 and 830 nm) and grouping B (780 and 830 nm). Simulated noise of approximately 0.5% with respect to the measured fluence Φ was added to the simulated measurements.

An example comparison of the reconstructed HbO₂ and HbR images is shown in Fig. 1 using wavelength grouping B (780 and 830 nm). Since the regularization parameter could affect the resolution of the two different imaging procedures differently, we altered the regularization parameter for each to equalize the full width at half-maximum (FWHM) of the reconstructed HbR object. In the indirect method, we used the same regularization parameter for each wavelength. For the case in Fig. 1, $\alpha = 0.01$ for the indirect reconstruction and $\alpha = 0.0025$ for the direct reconstruction. The direct concentration reconstruction has fewer and smaller artifacts and less cross talk as evidenced by the large decrease in HbO₂ in the indirect reconstruction in the center image slice that corresponds with the location of the true increased HbR.

To compare the two algorithms more quantitatively, we calculated the contrast-to-noise ratio (CNR) and cross talk of HbR into HbO₂ given a set of regularization parameters ($\alpha \in [0.0001 \text{ } 10]$) for the different wavelength groupings. The CNR is given by the peak value of HbR divided by the mean standard deviation of each voxel in the image.

The mean standard deviation is the statistical result of 200 independent noise simulations for each regularization parameter. In Fig. 2(a) we plot the $\log_{10}(\text{CNR})$ versus FWHM. Generally, over a wide range of regularization parameters α , the direct concentration reconstruction has a better CNR than the indirect method. This improvement in the direct method is observed since for the indirect method the concentrations are subsequently found by differencing the absorption images while the image noise (resulting from the measurement noise) is uncorrelated and sums. This results in a significantly reduced CNR.

Figure 2 also indicates that the choice of wavelengths plays an important role in optimization of the CNR.¹⁰ The (690-, 830-nm) pair makes the reconstruction of [HbO₂] and [HbR] less sensitive to the measurement noise relative to the (780-, 830-nm) pair, which is consistent with previous findings.¹⁰ Figure 2(b) indicates that the direct reconstruction results in less cross talk between HbR and HbO₂, where cross talk is defined as the HbO₂ change divided by the change in HbR in the position of the known object. Cross talk in the estimate of the hemoglobin concentrations occurs when the wavelength-dependent

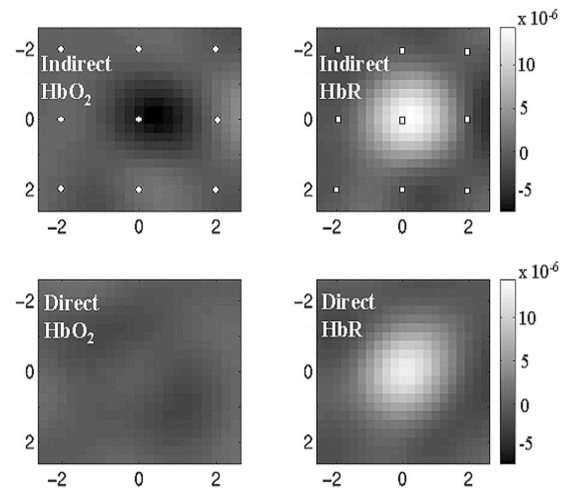


Fig. 1. Comparison of HbO₂ and HbR concentration reconstructions of simulated data by use of the indirect and direct methods. The field of view is 5 cm \times 5 cm, and in-depth center image slices are shown. The sources are at $z = 0$ and their xy positions are indicated by circles. The detectors are at $z = 6$ cm and their positions are indicated by squares.

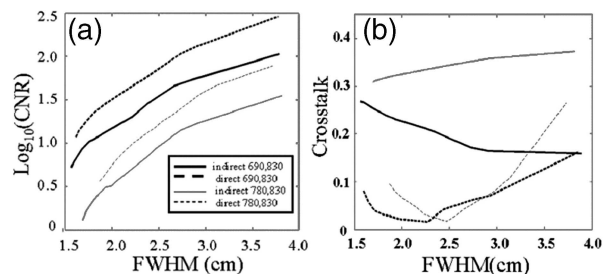


Fig. 2. Plotted are objective measures of the reconstructed images of simulated data of different wavelength combinations by use of indirect and direct methods: (a) CNR versus FWHM and (b) cross talk versus FWHM.

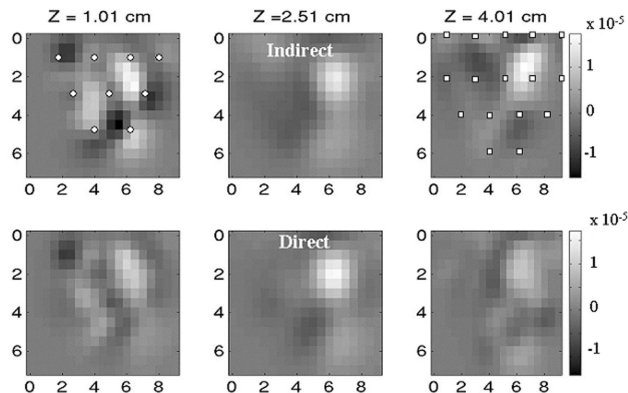


Fig. 3. Comparison of HbR concentration reconstructions of blood phantom experimental data by use of indirect and direct methods. The field of view is $10\text{ cm} \times 8\text{ cm}$, and image slices are shown at each 1.5-cm interval. The sources are at $z = 0$ and their xy positions are indicated by circles. The detectors are at $z = 5.5\text{ cm}$ and their positions are indicated by squares.

partial volume effect is incorrectly accounted for as described in Refs. 10 and 11. Thus cross talk in the indirect method should be reduced by matching as best as possible the point-spread function at each wavelength across the reconstruction volume. We tried this approach by finding different regularization parameters for the two wavelengths such that the FWHM at each wavelength matched the FWHM of the direct reconstruction of HbR. Interestingly, this did not produce a significant decrease in the cross talk observed with the indirect reconstruction, indicating that higher moments of the point-spread function difference across wavelengths produces the cross talk observed in the indirect reconstruction. Note that cross talk increases in the direct method as the FWHM increases above an optimal level, as one would expect given the increased blurring of the image. It is thus important to utilize the optimal regularization parameter as can be determined objectively from such a cross-talk analysis of the imaging matrix.

We performed the following blood phantom experiment to verify our simulation result. Our instrument is a continuous-wave imaging system that has two source wavelengths, 780 and 830 nm. The positions of the sources and detectors are shown in Fig. 3. The experiment employed a slab geometry with the nine sources and 16 detectors spread over a $10\text{ cm} \times 8\text{ cm}$ area on both the top plate (detectors) and the bottom plate (sources). The slab was 5.1 cm thick. A 0.5% Intralipid solution filled the tank as a background scattering medium. A 2-cm-diameter sphere was placed in the slab, with a center located at 6, 2, and 2.76 cm in X , Y , and Z coordinates, respectively. We mixed 50- μM pig blood with Intralipid and circulated it through the sphere. We took measurements as the blood converted from a fully deoxygenated state to a fully oxygenated state. We present the results of only the fully deoxygenated state. Before the blood was introduced into the sphere, we obtained a measurement of the homogeneous phantom for calibration purposes. Afterward, the deoxygenated blood was introduced into the sphere. The signal-to-noise ratio of the data

obtained with a 50-Hz bandwidth was 30–40 dB. The reconstructed images of the phantom data are shown in Fig. 3. The direct concentration reconstruction has a better CNR, fewer image artifacts, and reduced cross talk relative to the indirect method. Similar to the simulation, we calculated the CNR and cross talk for a set of regularization parameters ($\alpha \in [0.0001\ 10]$) using both algorithms on 200 independent experimental images. The calculation revealed that the improved CNR and reduced cross talk of the direct concentration algorithm are achieved over the range of the chosen regularization parameters. Note that, although the peak concentration is lower than expected because of image blurring, the integrated concentration over the volume of the object is conserved.

In conclusion, we introduced an algorithm that directly reconstructs images of the concentration of HbO₂ and HbR using multiple wavelength data. We showed and explained that this direct imaging approach significantly improves the image contrast-to-noise ratio and reduces the cross talk over the more traditional approach of reconstructing each wavelength separately and then converting the wavelength images to concentration images. The extension to direct imaging of other chromophores as well as a spectroscopic model for the scattering is straightforward. Further research is required to better understand the improvement in image quality when more wavelengths are used.

This research was funded in part by Advanced Research Technologies, NIH R01-CA97305, and by CenSSIS, the Center for Subsurface Sensing and Imaging Systems, under the Engineering Research Centers Program of the National Science Foundation, award number EEC-9986821. A. Li's e-mail address is angli@nmr.mgh.harvard.edu.

References

1. B. W. Pogue, S. P. Poplack, T. O. McBride, W. A. Wells, K. S. Osterman, U. L. Osterberg, and K. D. Paulsen, *Radiology* **218**, 261 (2001).
2. D. J. Hawrysz and E. M. Sevick-Muraca, *Neoplasia* **2**, 388 (2000).
3. S. R. Arridge, *Inverse Probl.* **15**, R41 (1999).
4. E. M. C. Hillman, "Experimental and theoretical investigations of near infrared tomographic imaging methods and clinical applications," Ph.D. dissertation (University College London, London, England, 2002).
5. T. Durduran, R. Choe, J. P. Culver, L. Zubkov, M. J. Holboke, J. Giammarco, B. Chance, and A. G. Yodh, *Phys. Med. Biol.* **47**, 2847 (2002).
6. A. Corlu, T. Durduran, R. Choe, M. Schweiger, E. M. C. Hillman, S. R. Arridge, and A. G. Yodh, *Opt. Lett.* **28**, 2339 (2003).
7. K. D. Paulsen and H. Jiang, *Med. Phys.* **22**, 691 (1995).
8. M. S. Patterson, B. Chance, and B. C. Wilson, *Appl. Opt.* **28**, 2331 (1989).
9. B. W. Pogue and M. S. Patterson, *Phys. Med. Biol.* **39**, 1157 (1994).
10. G. Strangman, M. A. Franceschini, and D. A. Boas, *Neuroimage* **18**, 865 (2003).
11. K. Uludag, M. Kohl, J. Steinbrink, H. Obrig, and A. Villringer, *J. Biomed. Opt.* **7**, 51 (2002).